CERN/PS/88.69(AR)

Theoretical Antiproton Yields for the AAC

Nicholas J Walker

CERN, Geneva, Switzerland.

November 3, 1988

Abstract

Antiproton yields into the Antiproton Collector ring (AC) of the Antiproton Accumulator Complex (AAC) have been calculated using a montecarlo approach. The target (antiproton production) and initial collecting lens have been modelled using a computer program written by Sherwood and Hancock (TGTST), which is based on an original program by van der Meer [1]. The model includes reabsorption and coulomb scattering of the antiprotons by the target and lens materials. The injection line is modelled by a particle tracking program (TERRAPIN), which includes multiple coulomb scattering of the beam by the air in those sections not under vacuum. Yields are reported for various types of collector lens and injection line optics. A simple analytical model of a linear lens is reported, in order to produce a clearer understanding of how the lens parameters (such as current and length) affect the yield.

1. INTRODUCTION

The antiproton yield into the Antiproton Collector (AC) ring of the new Antiproton Collector Complex (AAC) is dependent on many things: the characteristics and quality of the initial 26 GeV production beam, target material and length, optical and material properties of the collecting lens, beam optics of the injection line, and ultimately the particle losses in the AC itself are a few of the major factors. Previous calculations [2] have adopted a montecarlo approach to antiproton production in the target, and to ray tracing through the initial focusing lens. A computer model developed by Sherwood and Hancock, based on an original code by van der Meer [1] (hereafter referred to as TGTST), has been used extensively to model antiproton production, and scattering and reabsorption in the target and collector lens. TGTST generates antiprotons from a defined 26 GeV proton production beam, assuming antiproton production cross sections and production angle distributions from fitted available experimental data. The momentum distribution is considered to be flat over $\pm 3\%$ about the central momentum of the AC (3.5752 GeV/c), which is the momentum acceptance of the machine. The yield was calculated by counting the number of particles which fell into the AC transverse phase space acceptance ellipse, projected back through the injection line to the lens. Estimates were then made of the reduction of the yield due to various loss mechanisms, based on the difference between the observed and calculated yields made for the original Antiproton Accumulator (AA). The numbers reported in the literature[2] have always been quoted in terms of some reference or normalized value; this has lead in some cases to ambiguities when discussing the various calculated yields. It is therefor the subject of this report to try and clarify these ambiguities, by expanding the already existing montecarlo model to include the injection line, and hence calculate the yield directly into the AC. In this way, antiproton losses in the injection line due to gas scattering and chromatic effects can be included.

The montecarlo approach is generally the most flexible way of calculating the antiproton yield (although yields have been calculated using an analytical approach[3]), but from the point of view of lens design, it fails to give a clear understanding of how the optical parameters of the lens affect the yield. A simple linear optics method is used here to give analytical solutions to the problem of lens design. In the light of the pursuit of increased yields, this approach, although by no means exact, gives a useful guide to the type of specification required to obtain the maximum yield possible (taking into account engineering and financial constraints), and gives a useful starting point for the montecarlo calculations.

2. MONTECARLO SIMULATION OF ANTIPROTON PRODUCTION

In order to calculate the optimum parameters for a collecting lens, it is necessary to first model the distribution of antiprotons in four dimensional transverse phase space. The first stage (target stage) of TGTST generates a file of phase space coordinates of antiprotons at the exit of the target, which can be analyzed independently of the rest of the program. The target is modelled as a cylinder of a given material (in this case, either copper or iridium), surrounded by graphite. The model takes into account coulomb scattering of the antiprotons as they are tracked through the target, as well as reabsorption. Figure 1 shows a typical phase space distribution produced by a 60x3mm iridium target, for 26 GeV proton production beam with a diameter of 1mm diameter (corresponding to an emittance of 0.42π mm.mrad) at the entrance of the target.

Ignoring second order (nonlinear) effects, the maximum yield into the AC is obtained by matching the machine acceptance through the injection line and collector lens, to an ellipse at the end of the target which contains the maximum number of particles. The ellipse drawn in figure 1 represents the maximum yield for an acceptance of 200π mm.mrad in both planes. It is clear that a lens would have

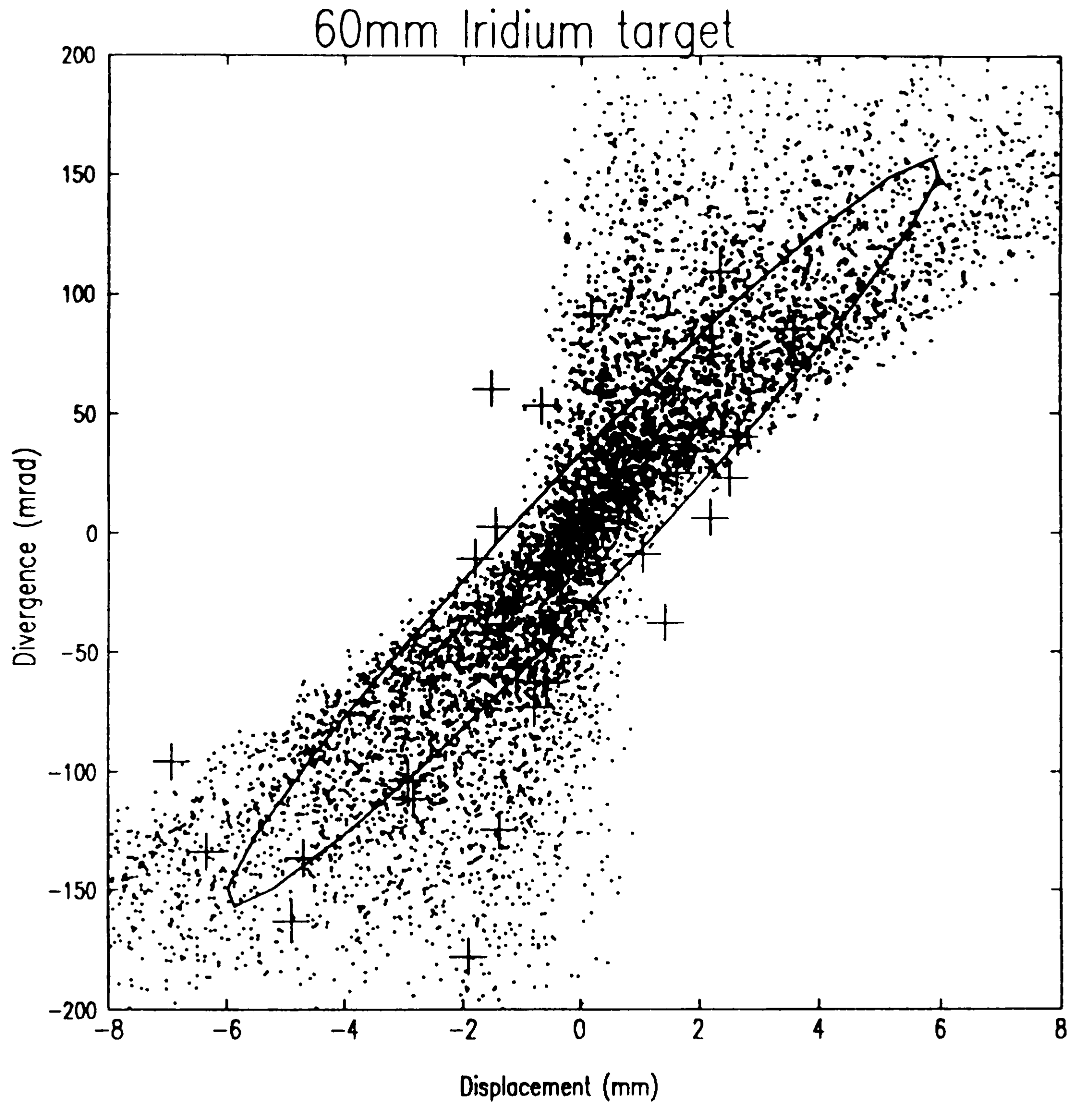

Figure 1: Distribution of antiprotons in phase space at the end of the target. The . represent antiprotons born in the target, while the + represent those antiprotons born in the surrounding graphite.

to focus particles with angles up to approximately 140 mrad in order to obtain the maximum yield into 200π mm.mrad; this is generally not possible due to either engineering or financial constraints (or both). Instead, a compromise between the best yield and what is practically and economically possible is required. Figure 2 shows the normalized yield as a function of maximum divergence (θ) for various targets. The graph was produced by fixing the value of θ and varying the maximum displacement of the constant area ellipse until a maximum yield was obtained. In general, this ellipse will be tilted; this enables the definition of a centre of production, i.e. that point a distance d upstream of the exit of the target, where the ellipse is upright (see figure 3). The mean values of d are given in table 1, and are important when considering the linear lens parameters (see section 3).

Table 1: Values of d for various targets

target	length (mm)	d (mm)
Iridium	60	36
Iridium	30	16
Copper	60	30
Copper	30	16

The results shown in figure 2 lead to two general conclusions: a) as the angle increases, the yield also increases until a value of about 150 mrad, at which point no further gain is made, and b) higher angles favor shorter targets. The first point is simply explained by the production angle distribution function, which is built into the model, and peaks at about 150 mrad. The second point is due to a depth of field effect; as the ellipse becomes narrower at the centre of production (corresponding to larger value of θ, and consequently a smaller width in displacement), only those antiprotons generated in a shorter target length fall into the acceptance.

Having found the best ellipse shape at the exit of the target, it is now necessary to see how the various lens parameters can be made to match this into the injection line.

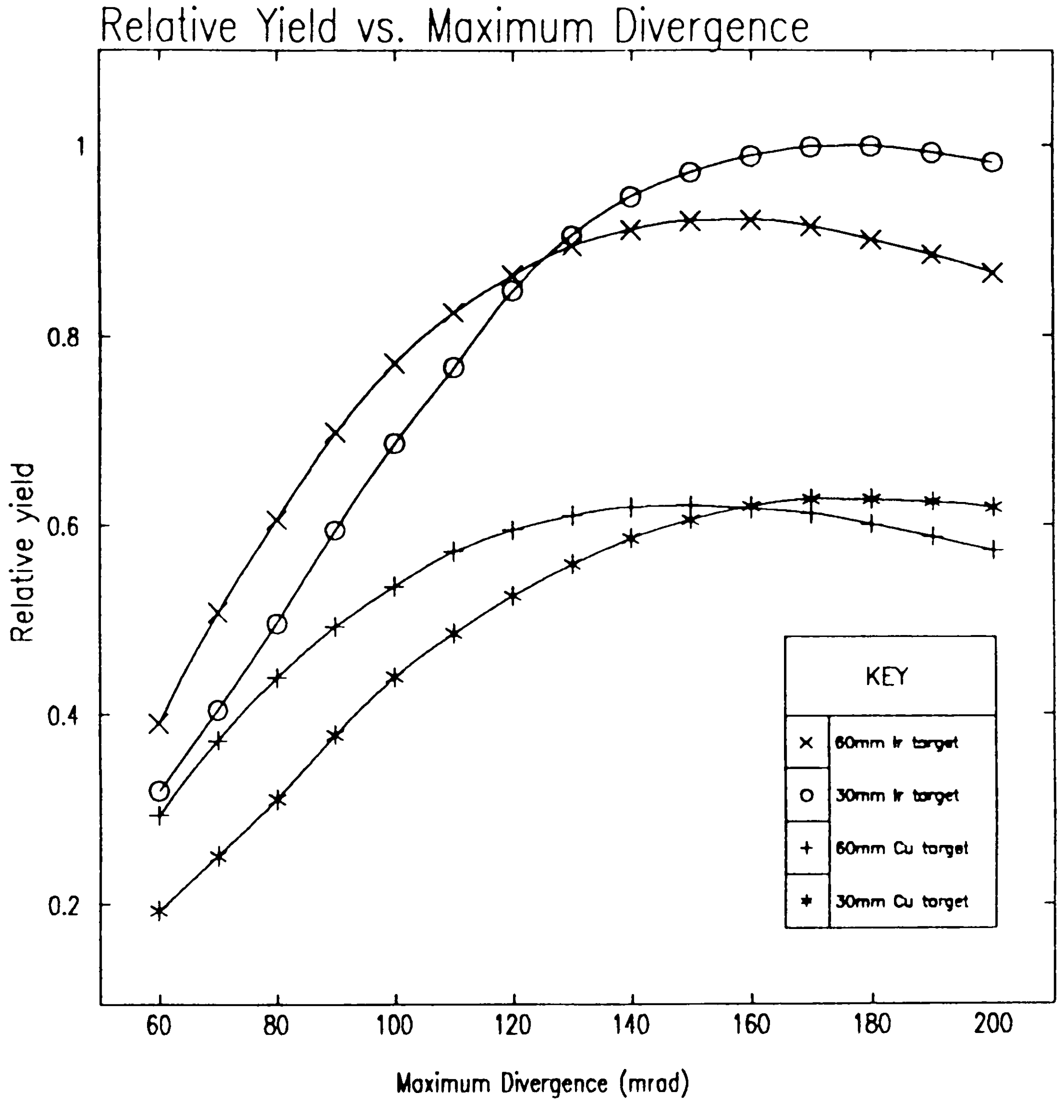

Figure 2: Normalized yield versus maximum divergence. The graph shows the yield (normalized to the maximum yield calculated) for four types of target, as a function of maximum divergence.

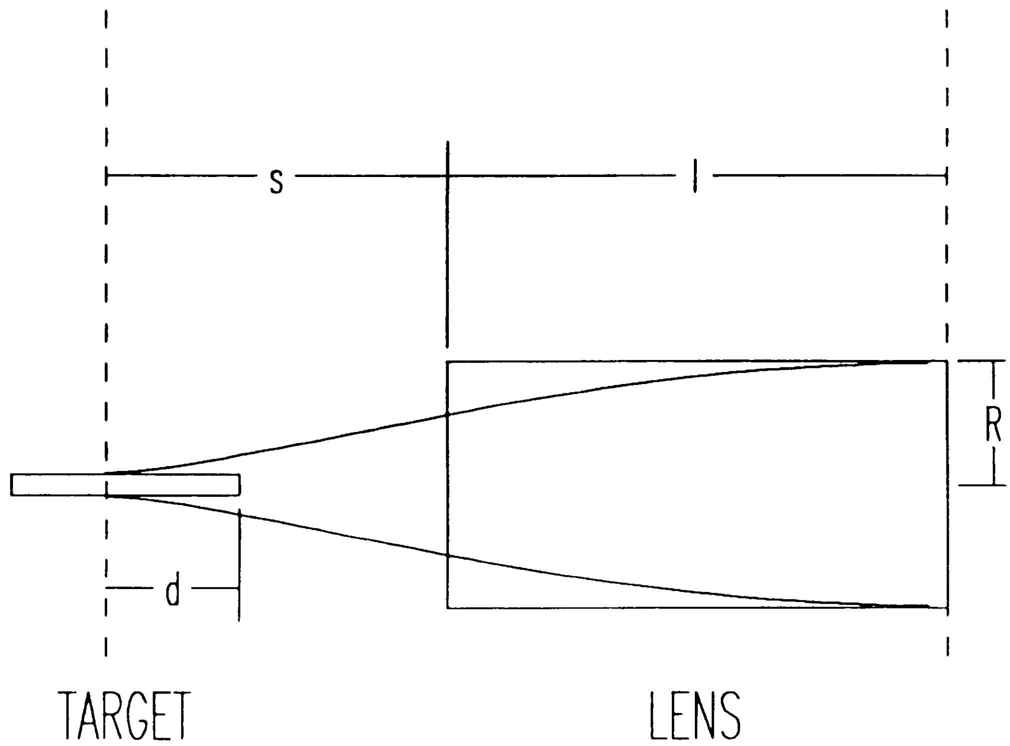

Figure 3: Target lens geometry for linear optics calculations

3. LINEAR LENS OPTICS.

A *linear* lens is defined as one in which the field is proportional to the radius. In all the cases discussed here, it is assumed to be a current carrying cylinder with a uniform current density. In order to define the specification for a lens, it is first necessary to understand how the various free design parameters (for example lens current and radius) relate to the projected phase space ellipse at the centre of production of the target. If we define the Courant and Snyder parameters upstream of the lens by (α_0, β_0, γ_0), and at the exit of the lens by (α_1, β_1, γ_1), then:

$$\begin{vmatrix} \beta_1 \\ \alpha_1 \\ \gamma_1 \end{vmatrix} = \begin{vmatrix} (\cos\psi - sk\sin\psi)^2 & (s^2k - \frac{1}{k})\sin2\psi - 2s\cos2\psi & (\frac{1}{k}\sin2\psi + s\cos\psi)^2 \\ \frac{k}{2}\sin2\psi - sk^2\sin^2\psi & \cos2\psi - sk\sin2\psi & -\frac{1}{2k}\sin2\psi - s\cos^2\psi \\ k^2\sin^2\psi & k\sin2\psi & \cos^2\psi \end{vmatrix} \begin{vmatrix} \beta_0 \\ \alpha_0 \\ \gamma_0 \end{vmatrix} \qquad (1)$$

where $\psi = kl$, and $k^2 = \frac{1}{B\rho}\frac{\partial B}{\partial r}$. The transfer matrix is simply $R_{quad} \times R_{drift}$. Again due to the cylindrical symmetry, only one plane need be considered. Defining $\alpha_0 = \alpha_1 = 0$, equation (1) can generate two useful equations:

$$\beta_0 = (\cos\psi - sk\sin\psi)^2\beta_1 + (\frac{\sin\psi}{k} + s\cos\psi)^2\frac{1}{\beta_1} \ , \qquad (2)$$

$$0 = \frac{1}{2}(k\beta_1^2 - \frac{1}{k})\sin2\psi - s[(\beta_1 k\sin\psi)^2 + s\cos^2\psi] \ . \qquad (3)$$

By reversing the order of drift and lens matrix ($R_{drift} \times R_{quad}$), two more equations can be obtained in a similar way:

$$\beta_1 = \beta_0\cos^2\psi + (s\cos\psi + \frac{1}{k}\sin\psi)^2\frac{1}{\beta_0} \ , \qquad (4)$$

$$0 = \frac{1}{2}(k\beta_0^2 + s^2k - \frac{1}{k})\sin2\psi - s\cos2\psi \ . \qquad (5)$$

The five parameters which appear in equations (2−5) (β_0, β_1, k, ψ, s) are directly related to the five lens parameters, defined as:

1. Length $l = \frac{\psi}{k}$,
2. Radius $R = \sqrt{\beta_1\varepsilon}$,
3. Current $I = \frac{2\pi\rho B}{\mu_0}R^2k^2$,
4. Lens to waist distance s,
5. Maximum collection angle $\theta_{max} = \sqrt{\frac{\varepsilon}{\beta_0}}$.

Figures 4 and 5 show the solutions equations (2) and (3) for two lens diameters (10 mm and 36 mm respectively). The graphs show the accepted production angle (θ_{max}) for various lengths of lens, with the independent variable chosen as lens current, since this is probably the most important parameter from a practical engineering point of view. The dotted lines indicate the lens to drift distance, s. The choice of a real lens is severely restricted by s, since the engineering constraints, together with the fact that this distance must include a certain amount of the target length (see figure 3), generally means that s cannot be less than 100 mm. This tends to favor a larger diameter lens. Larger currents are also generally required (typically in the order of 1 MAmp) in order to focus a larger angle, and hence give an increased yield.

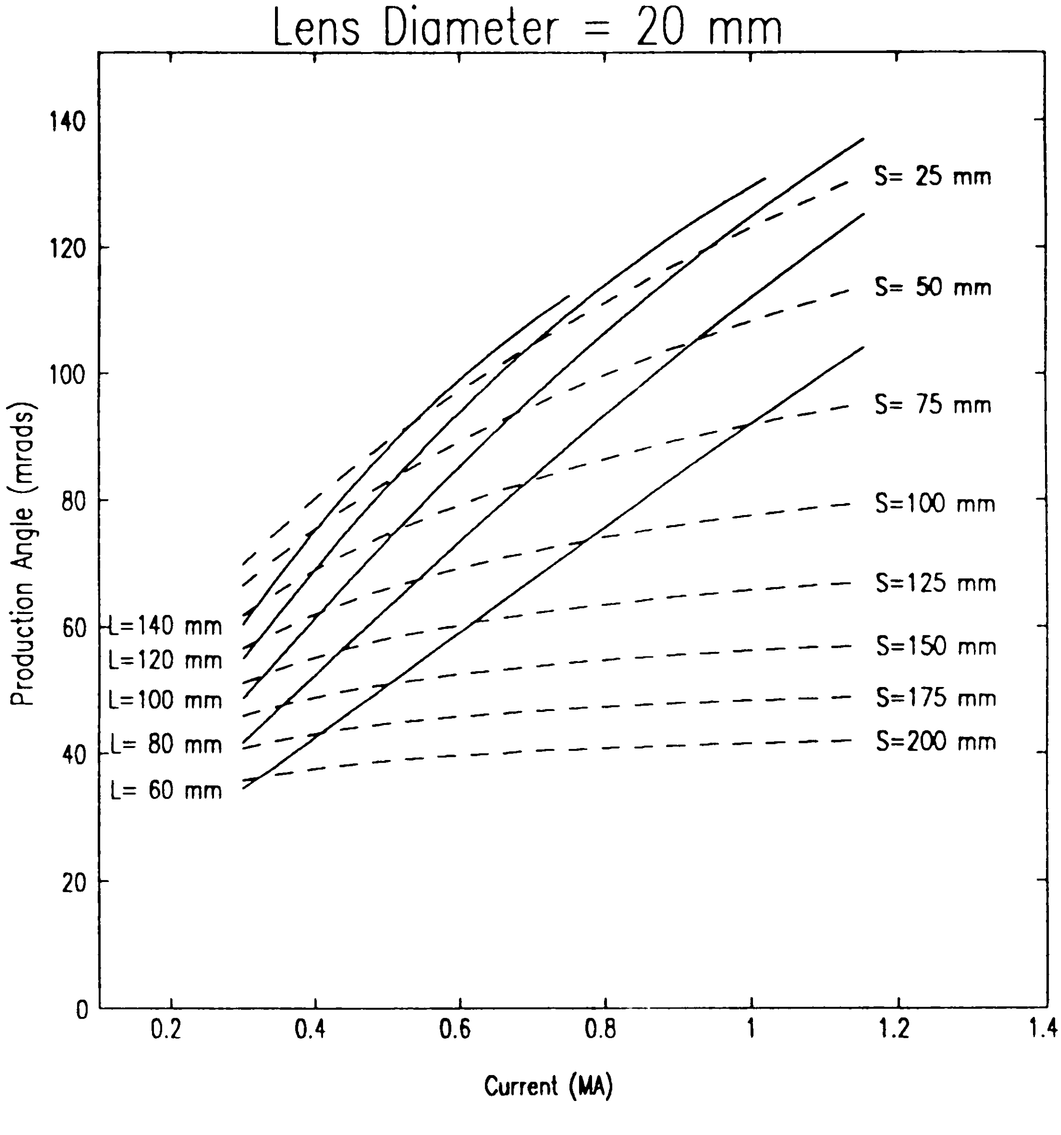

Figure 4: Linear lens parameters for a 20mm diameter lens

Another possible criterion for the choice of a lens is that of chromatic aberration. All the previous calculations were done assuming particles with a magnetic rigidity corresponding to a momentum of 3.5752 GeV/c, the central momentum of the AC. However, due to the large momentum spread of 6% accepted by the machine, chromatic effects could become important, and for certain cases produce a significant reduction in the yield. To investigate the effect, the Courant and Snyder parameters of a beam with a momentum of +3% were calculated for a given matched solution for a lens.[1] The frac-

[1] By matched, we mean an exact solution to equations 2 and 3.

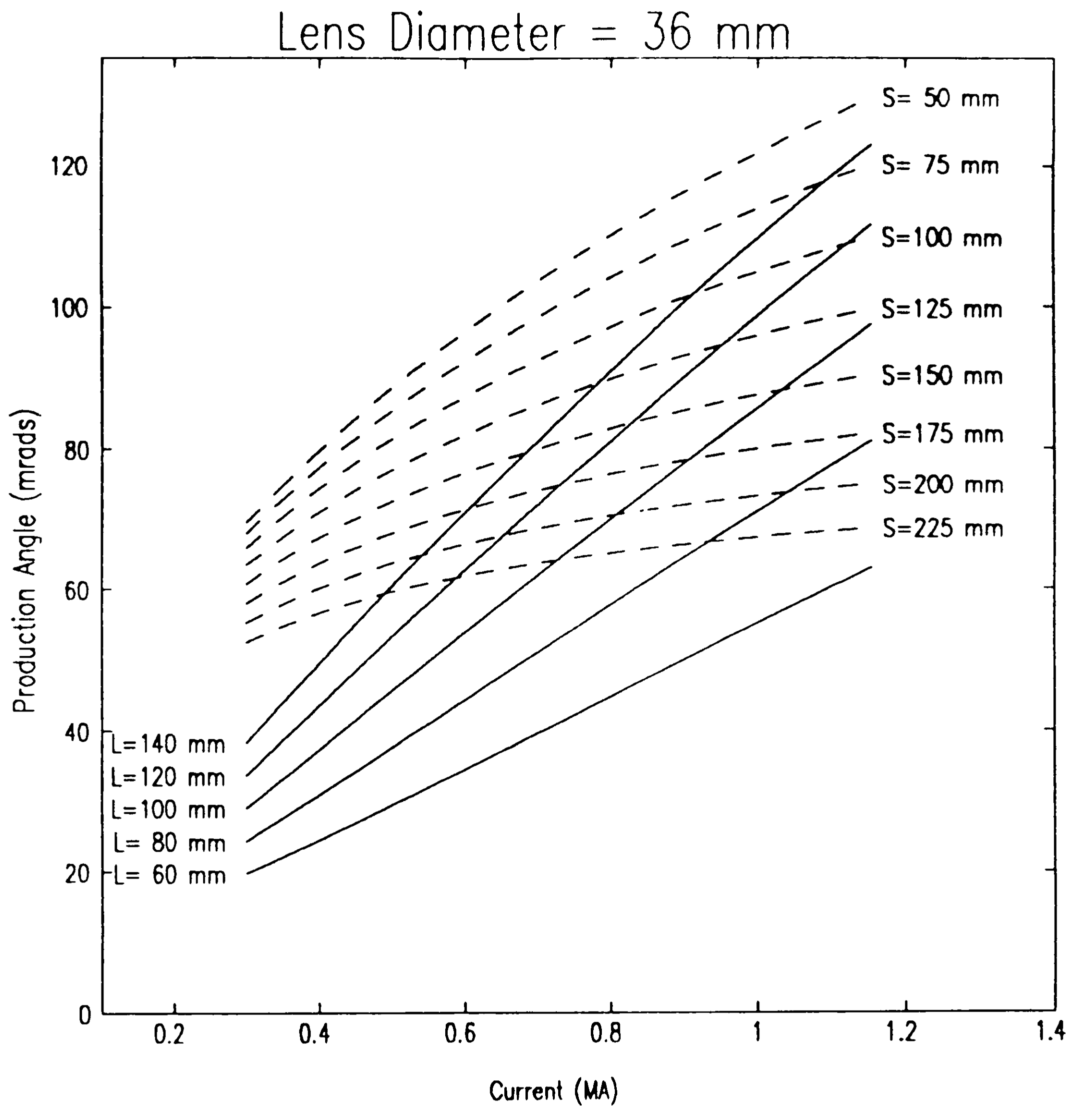

Figure 5: Linear lens parameters for a 36mm diameter lens

tion of common area of this and the matched ellipse, calculated from

$$\frac{4}{\pi}\tan^{-1}\left|\left(D-\sqrt{D^2-1}\right)^{\frac{1}{2}}\right| \qquad (6)$$

where

$$D=\frac{1}{2}\left(\frac{\beta_2}{\beta_1}+\gamma_2\beta_1\right)$$

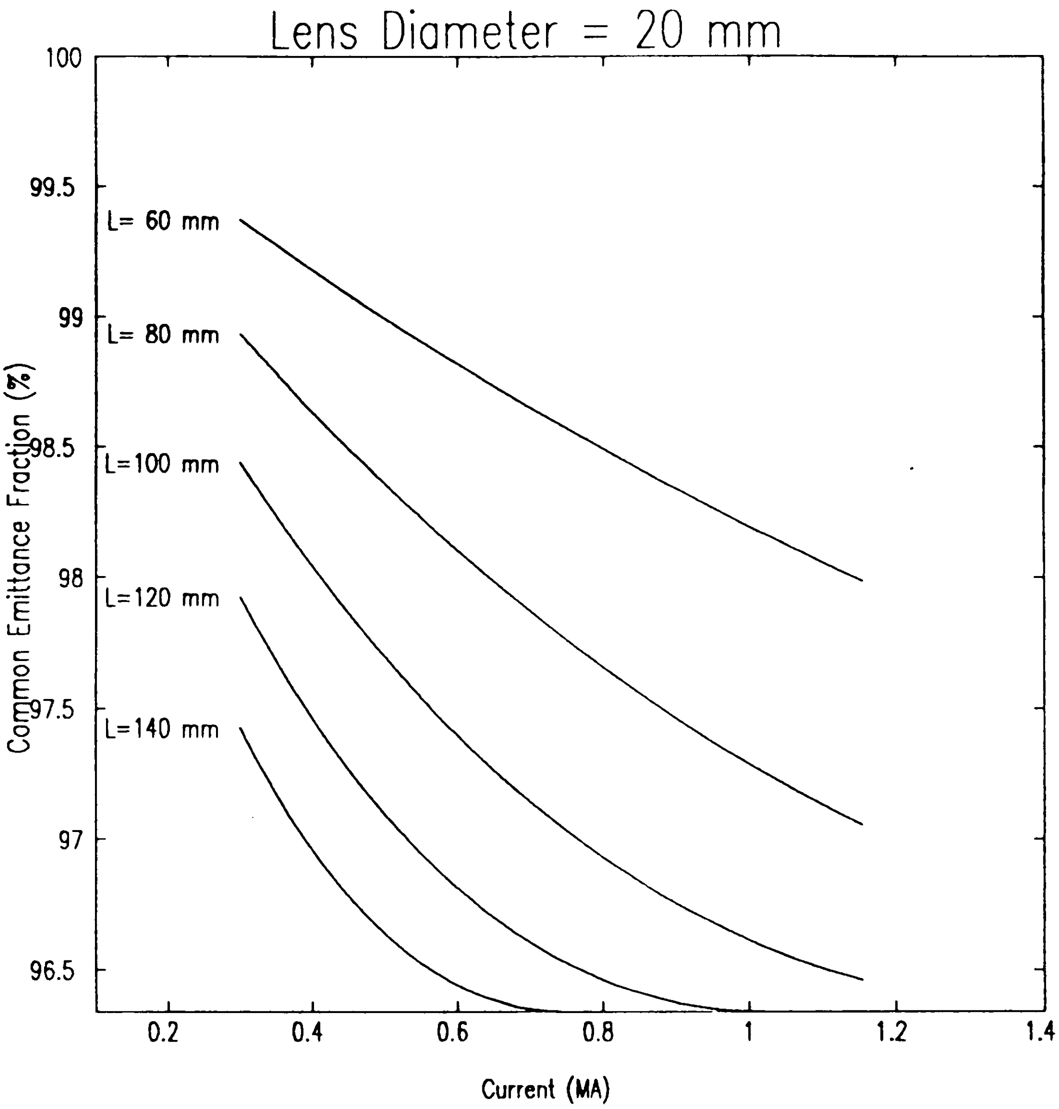

Figure 6: Chromatic effects for a 20mm diameter linear lens

where the subscript 2 corresponds to the ellipse for the $+3\%$ case, are shown in figures 6 and 7. The results indicate that a long high current lens has the worst dispersion, but this effect is still small (typically a few percent), and so can generally be neglected.

Although the families of curves presented in figures 4 and 5 give a good analytical solution to the design problem of a linear lens, they do not take into account the problems of scattering and reabsorption of antiprotons in the material of the lens itself. Also, this approach cannot be used in the case of a nonlinear focusing lens, such as a magnetic horn. In these cases, a ray tracing montecarlo type approach must be used, such as that adopted by TGTST, already mentioned in conjunction with antiproton production in the target (section 2).

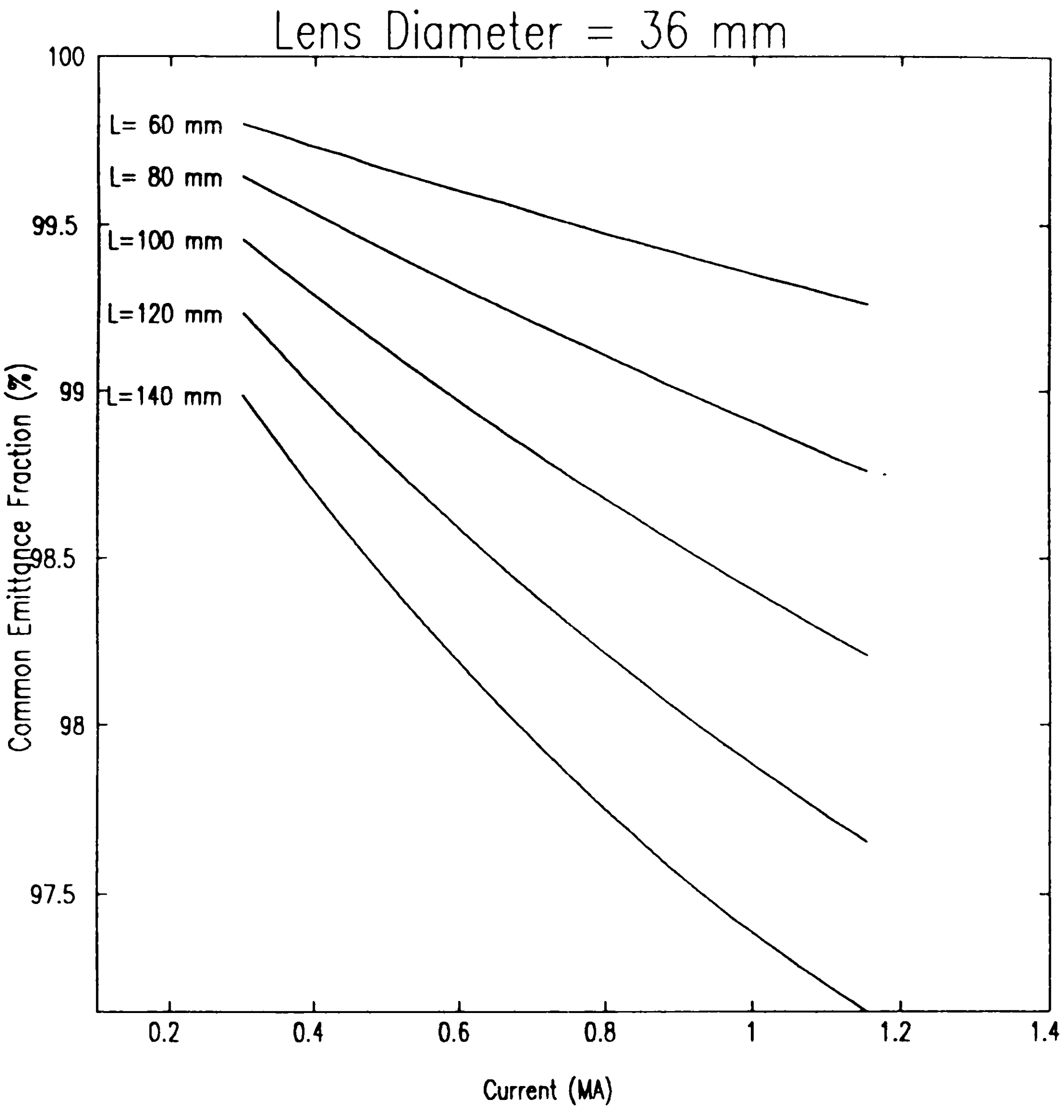

Figure 7: Chromatic effects for a 36mm diameter linear lens

4. MONTECARLO SIMULATION OF THE COLLECTING LENS.

The effect of coulomb scattering, together with reabsorption of the antiprotons will become more pronounced as the lens becomes longer. Figure 8 demonstrates this effect by plotting yield[2] against lens length for various lens materials. In all cases, the lens current was fixed at an arbitrary value of 1 MAmp, with a diameter of 36mm, and the value of the drift distance, s, was adjusted for each value of length to provide a matched situation. The solid line was calculated from the linear lens optics pre-

[2] In all cases, the term yield refers to the number of antiprotons per proton on target.

sented in the previous section. In all other cases, the yield is calculated using TGTS1. The graph for the plasma lens is a montecarlo calculation with the scattering and reabsorption turned off (i.e. each particle produced by the target is simply ray traced through and up to the exit of the lens). It is clear from these results that the effect of the scattering and reabsorption is quite considerable. For example, although the solid line shows that an increase in yield can be gained by going to a longer lens, the effect of the scattering and reabsorption is such that, in the case of a lens fabricated from aluminum, there is a decrease in yield with lengths greater than 140mm. It is difficult to include the magnetic horn in this type of comparison due to it's nonlinear nature, since it is impossible to make all other parameters equal. The effect of the scattering will not, however, be negligible (see section 6).

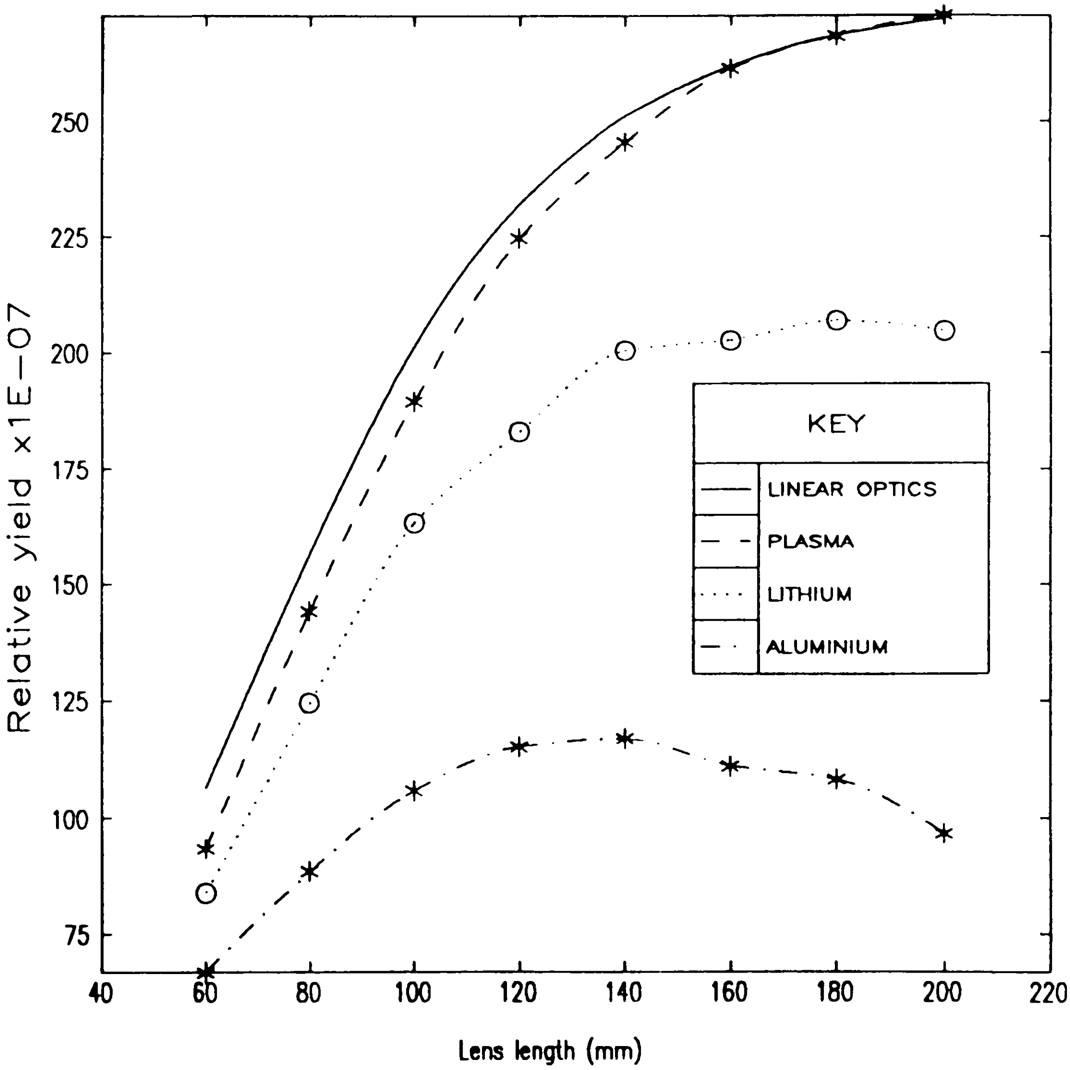

Figure 8: Effect of coulomb scattering and reabsorption on yield. The graphs show the yield as a function of lens length for various lens materials. The solid line represents that yield calculated from linear optics. In all cases, the current is 1 MAmp.

5. PARTICLE TRACKING THROUGH THE INJECTION LINE.

In previous yield calculations [2], the results presented were obtained directly from TGTST, that is the yield was calculated by counting the number off particles that fell into a defined acceptance at the exit of the collector lens. For a more precise calculation of the antiproton yield in the AC, it is necessary to extend the montecarlo approach of TGTST to include particle tracking through the injection line and into the machine itself. To facilitate this, a small particle tracking program called TERRAPIN has been written, which enables the file of particle phase space coordinates produced at the exit of the lens to be tracked into the AC. TERRAPIN tracks each particle in turn through the various elements, taking into account all the physical apertures. It also models the effect of the coulomb scattering due to the air in the injection line, which generally causes a reduction in the yield. Although TERRAPIN is first order in terms of transport matrices[4] , the program takes into account chromatic aberration at the quadrupoles, which appears to be the most significant second order effect [5].

The original design of the injection line was based on the use of a 36mm diameter lithium collecting lens, as defined in the AAC design report [6]. The optics (hereafter referred to as optic 1) was calculated to match a 240π mm.mrad machine ellipse to the radius of the lens, while correcting the large dispersion of the spectrometer (dogleg) to match the zero dispersion of the AC[3] [7]. Later it was clear that this lens was not feasible for the start up of the AAC, and it was necessary to try and find a solution to match for the smaller 20mm diameter lithium lens (optic 2). A further solution was required for the 60mm diameter 400 kAmp magnetic horn (optic 3). In both cases, it was impossible to match the lens radius to the machine ellipse for 240π mm.mrad due to the aperture restrictions of the injection line, while maintaining the original design geometry and preserving the correct momentum collimation in the spectrometer. Instead a compromise was arrived at, whereby an ellipse at the exit of the lens could be matched into the AC for an emittance of 200π mm.mrad [8]. In the case of the ϕ20mm lithium lens, the best solution was an upright ellipse at the exit of the lens, with a radius of 15mm (corresponding to $\beta = 1.125$m), slightly larger than the lens radius. For the 60mm magnetic horn, it was not possible to find a solution with an upright ellipse, and so a tilted ellipse with a radius of 30mm ($\beta = 4.5$m) and $\alpha = -0.382$ was used. All three of these optics are summarized in table 2, and the beam envelopes (calculated using TERRAPIN) are given in appendix A, for values of $\Delta p/p$ of 0% and ± 3%. It should be noted that the beam envelopes do in fact clip the magnet and vacuum pipe apertures in several places; this is due to the chromatic effects at the quadrupoles, an effect not taken into account in first order transport calculations.

---

[3] A match was attempted to first order such that the beam envelope defined for a given emittance fitted within all aperture restrictions in the injection line.

Table 2: Injection line optics.

The table shows the matched ellipse parameters at the exit of the lens for each of the optics solutions referred to in the text. $R = \sqrt{\beta\varepsilon}$ and $\theta = \sqrt{\gamma\varepsilon}$.

optic	ε (mm.mrad)	β (m)	α	R (mm)	θ (mrad)
1.	240.π	1.35	0.0	18.0	13.333
2.	200.π	1.125	0.0	15.0	13.333
3.	200.π	4.5	− 0.382	30.0	7.141

6. ANTIPROTON YIELDS.

Using TGTST in conjunction with TERRAPIN, it is now possible to calculate the antiproton yield into the acceptance of the AC, defined at the centre of quadrupole QDN01. TGTST generates a file of particle phase space coordinates st the exit of the target, as well as at the exit of the lens. Thus it is possible to analyse the yields at each stage, and make a comparative assessment of the antiproton losses at each point of the model. The following types of lens have been investigated:

1. 150mm x ϕ36mm lithium lens,

2. 150mm x ϕ20mm lithium lens,

3. 100mm x ϕ20mm lithium lens,

4. 80mm x ϕ36mm aluminium alloy lens,

5. 70mm x ϕ20mm aluminium alloy lens,

6. ϕ60mm (400 kAmp) parabolic magnetic horn.

Both the 150xϕ20mm lithium lens and the ϕ60mm (400kAmp) magnetic horn have been used for antiproton production. The 20mm diameter lithium lens [9] was used during the commissioning of the AAC in the latter part of 1987, and is presently being used. The 400 kAmp horn [10] was used for a trial period in April 1988. Although plans for the 36mm lithium lens were originally delayed due to financial reasons, plans for a 1300 kAmp[4] pulser for such a lens are presently being made in collaboration with the Institute of Nuclear Physics, Novosibirsk[11]. Table 3 gives the current (I) and lens target separation[5] (Z) for each lens. Care has been taken that the engineering constraints of the various lenses have not been exceeded; maximum currents and minimum target to lens separations have been used where such data is available. Because of these restrictions, not all the lens configurations are at their optimum. The value of Z for the 150xϕ20mm lithium lens, for example, is too high, and the

4 This value refers to the *peak* current, not the d.c. equivalent current used in the simulations.

5 Here, the lens target separation is defined as the distance between the exit of the target and the upstream end of the lens.

optimum position for the target would be some 20mm closer to the lens. The shorter 150xϕ20mm lithium lens was proposed as a possible solution for an optimum configuration. The aluminium alloy lens was first proposed as a cheap engineering solution to the lithium lens problem, and consists of a coaxial structure of insulated concentric cylinders, which enable a reduction in the time required for current penetration [12]. The lithium lenses are modelled as a cylinder surrounded by an iron transformer core, in which the field is assumed to fall off as 1/r. In the case of the aluminium lens, the coaxial structure means that the lens (the inner conductor) is surrounded by the outer return current path, which is made of the same material. Because of the reverse current flow outside the lens, the field falls off as $(R^2/r - r)$ where R is the total radius of the lens (including return current path). The material for the lenses are actually aluminium alloys, (for the 36mm diameter lens, the alloy is 91.65% Al, 4.5% Mg, 0.7% Mn and 0.15% Cr, while for the 20mm diameter lens, it is 86.7% Al, 2.5% Mg, 1.6% Cu, 0.23% Cr, and 5.6% Zn). The radiation and absorption lengths for these alloys were calculated as a weighted average of the recipricol length of each element present. The current used in the calculation was obtained from the theoretical value of the most linear field for the lens (1500 Tm^{-1} and 833 Tm^{-1} for the 20mm and 36mm diameter lenses respectively) [12].

Table 3: Lens Parameters for Maximum Yield

The following table gives the values of lens current (I) and target lens separation (Z) used in the yield calculations. Attention has been payed to possible engineering constraints, and these are noted in the last column.

Lens	Z (mm)	I (kAmps)	Comments
Li ϕ36x150mm	80	970	Min. Z, opt. I
Li ϕ20x150mm	50	380	Min. Z, max. I
Li ϕ20x100mm	50	485	min. Z, opt. I
Al ϕ20x70mm	42	750	Opt. Z, calc. I (see text)
Al ϕ36x80mm	115	1350	Opt. Z, calc. I (see text)
Al horn ϕ60mm	175	400	Opt. Z, max. I

In the case of the lithium lenses, there are windows at both ends of the lens which are required to be mechanically strong to withstand the magnetic pressure. These windows will increase the scattering and absorption of the beam, and so must be taken into account by the model. The effect of scattering is greater with a low divergence beam, such as that obtained at the exit of the lens. Thus only the scattering of the downstream window was considered, the effect of the entrance window being neglected. The exit window was modelled as 1cm of titanium using TERRAPIN, by defining it as the first element of the injection line. The effect of this window scattering is to generally reduce the yield by approximately 2%. Replacing the titanium by beryllium reduces this loss to 1.6%. The effect of the absorption is more severe. In the case of titanium, a further 7% of the antiprotons are absorbed in the window (in this case, both windows must be taken into account). Beryllium is slightly better at 5%.

Table 4 lists the results for the various lens and injection line optics combinations. In the case of the lithium and aluminium alloy lenses, both the 36mm (optic 1) and the 20mm (optic 2) optics were investigated. In all the cases, the lens parameters were adjusted to give the maximum yield into the acceptance *at the exit of the lens* (see table 3), defined for 200π mm.mrad in both planes. The file of particles thus produced were then used as the input for TERRAPIN in order to calculate the yield into the AC. The column headed Y1 in table 4 represents the maximum yield possible for a the given lens and optics; it is obtained using the montecarlo program, by calculating the yield into the acceptance at the exit of the lens, but with all the scattering and reabsorption in the lens itself turned off. This is the yield that could be achieved if all scattering, reabsorption and second order optical effects (eg. chromatic aberration at the quadrupoles) could be removed, and is used as a bench mark to gauge these effects. the yield given in Y2 is from the same calculation, but including the scattering and reabsorption. The figure in brackets represents the percentage loss due to these effects, as compared to Y1. Y3 and Y4 show the yields calculated into the AC using TERRAPIN. Y3 is calculated with no gas scattering in the injection line, while Y4 includes the scattering, and as such should be the true injected yield into the AC. Figure 9 gives the yield in the AC as a function of acceptance (assumed equal in both planes). The graphs reflect the results already presented in table 4.

Table 4: Antiproton Yield Analysis

The table below gives the theoretical antiproton yields (for 200π mm.mrad in both planes) for various collector lenses and injection line optics. All yields are relative to a production beam of 10^{13} protons ($\times 10^{-6}$), assuming a 60x3mm iridium target. The yields are as follows:

Y1 Yield into acceptance at exit of the lens. No scattering or reabsorption in the lens.

Y2 Same as for Y1, but includes the effects of scattering and reabsorption in the lens.

Y3 Yield into AC acceptance. Includes scattering and reabsorption in lens, but no gas scattering in injection line.

Y4 As for Y3, but now includes the air scattering.

The figures in the brackets represent the percentage of beam loss for each successive column, using Y1 as a reference. The last column is the total loss. With the lithium lenses, the figures for Y1 to Y4 include losses due to the two titanium windows, assumed to be 1cm thick.

Lens	optic	Y1	Y2	Y3	Y4	loss
Li ϕ36x150mm	1	19.7	15.1 (23%)	14.9 (1%)	13.7 (6%)	30%
Li ϕ20x150mm	2	16.3	10.6 (35%)	10.3 (2%)	9.7 (4%)	41%
Li ϕ20x150mm	1	16.1	10.6 (35%)	10.3 (2%)	9.7 (4%)	40%
Li ϕ20x100mm	2	16.6	12.0 (28%)	11.6 (2%)	10.8 (5%)	35%
Li ϕ20x100mm	1	16.0	11.6 (28%)	11.4 (1%)	10.7 (4%)	33%
Al ϕ36x80mm	1	17.5	13.2 (25%)	13.0 (1%)	12.0 (6%)	32%
Al ϕ20x70mm	2	15.3	11.6 (24%)	11.2 (3%)	10.6 (4%)	31%
Al ϕ20x70mm	1	14.9	11.1 (26%)	10.9 (1%)	10.8 (1%)	28%
Al horn ϕ60mm	3	16.1	12.7 (21%)	11.6 (7%)	10.7 (6%)	34%

The results presented in table 4 show that the highest yield would be obtained with the 36mm diameter lithium lens with a high current, a 40% increase over the present 20mm lithium lens or the 60mm horn. This is entirely in agreement with the linear optics calculations presented in section 3. The large loss due to scattering and absorption in the lithium lenses (Y2) are enhanced by the window effects, which contribute some 9% to the total loss. Making these windows thinner would increase the yield, and in fact in reality the windows are concaved, with an average thickness of 0.8cm. The losses for the aluminium lenses and horn are entirely due the material of the lens itself; this can only be reduced by using different alloys which are more transparant to the antiprotons, or by redesigning (in then case of the horn) to use less material. The losses due to the gas scattering in the injection line appear to be in the range of 6% to 8% (as compared to Y3). This appears to be a smaller effect than previously expected[5], but may be due to the fact that the yield is calculated into an AC acceptance of 200π mm.mrad. When using an acceptance of 240π mm.mrad, the effect is closer to 10% to 12%. The difference probably arises from the fact that it is the particles at high amplitude betatron oscillations that get lost due to scattering, so the effect becomes more pronounced as the acceptance is increased.

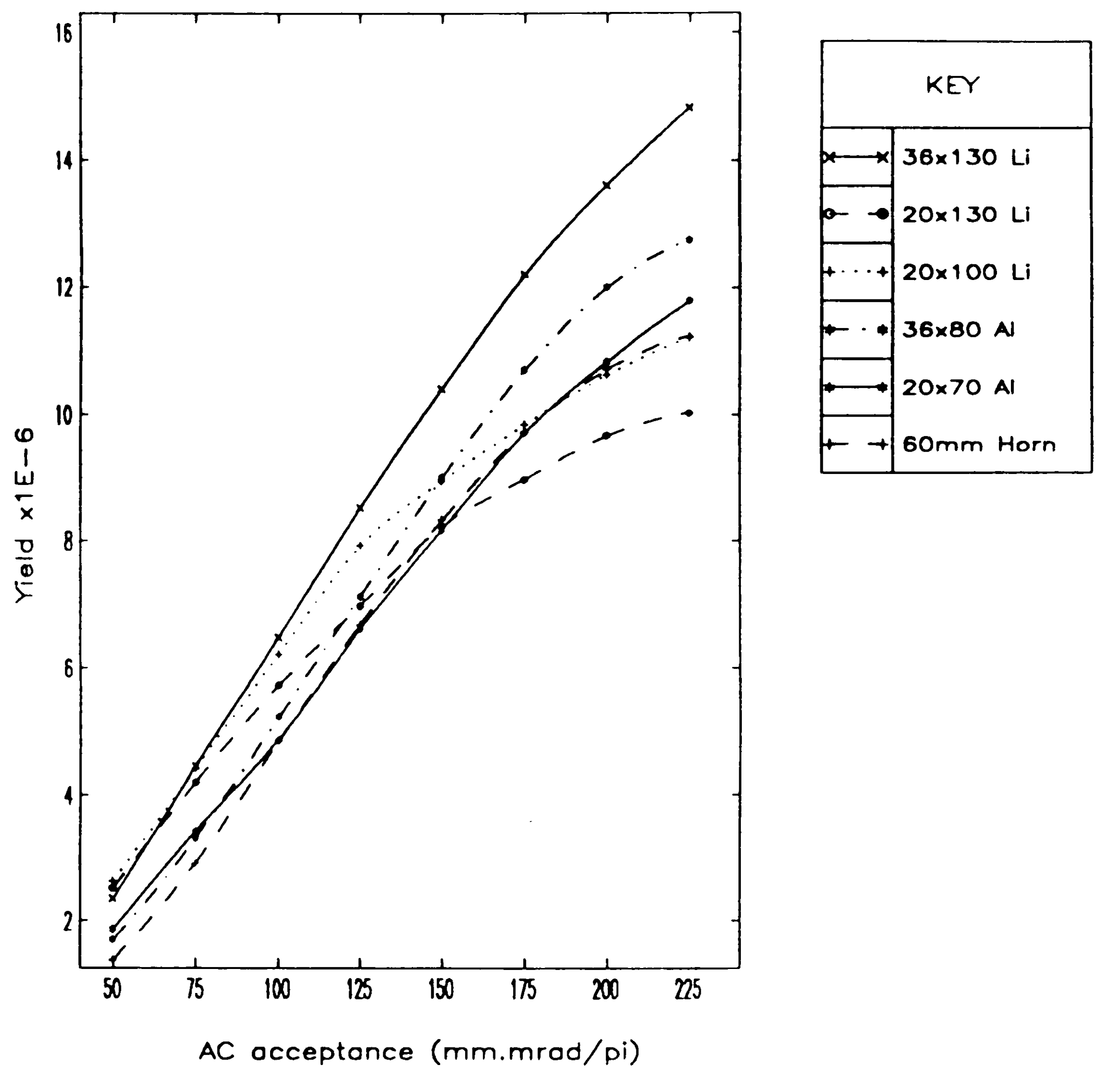

Figure 9: Antiproton yield as a function of AC acceptance. The graphs presented represent the yield as a function of AC acceptance (assumed equal in both planes), and into a *rectangular* aperture in real space. No corrections have been made for linear coupling or losses due to nonlinear resonances.

7. POSSIBLE SOURCES OF ANTIPROTON LOSS.

Experimental yield values are available for the 20x150mm lithium lens and the 60mm diameter, 400 kAmp magnetic horn[13]. The experimentally observed yield appears to be a factor of 1.5 – 2.0 down on those figures presented in table 4. A fraction of this difference may be accounted for by losses in the AC due to linear coupling and non – linear resonances, since the theoretical yield is only calculated into the acceptance of the AC defined at the centre of quadrupole QDN01. The acceptance of the AC is assumed to be the same ellipse for all momenta. In reality the acceptance will be different with a change in momentum, which almost certainly have an affect on the calculated yield.[14]

The effect of the vacuum windows in the injection line (which have been ignored here) will cause a further reduction in yield. These windows are, however, very thin (50μm of stainless steel), and the effect of losses due to scattering and absorption have been estimated to be of the order of 1%. Since the intrinsic statistical error of the calculation tends to put an uncertainty of approximately $\pm$5% on the quoted theoretical yields, this additional loss can be ignored. Finally, there is a small error in the physical model of absorption mechanism incorporated in TGTST. At present, the nuclear inelastic interaction length is used for the absorption length. This is the mean free path between nuclear interactions, which result in the absorption of the antiproton. It does not include the losses due to large angle (elastic) scattering of the antiprotons caused by 'billiard ball' type collisions with nuclei (this differs from the small angle coulomb scattering, which is electrostatic in nature). A more accurate description would be to use the nuclear collision length, which includes both elastic and inelastic collisions;. this may decrease the calculated yield by as much as 10%.

8. ACKNOWLEDGEMENTS.

I would like to thank C.D. Johnson, E. Jones, P. Krejcik and T.R. Sherwood for their help and many useful discussions.

Appendix A

BEAM ENVELOPES FOR THE INJECTION LINE OPTICS.

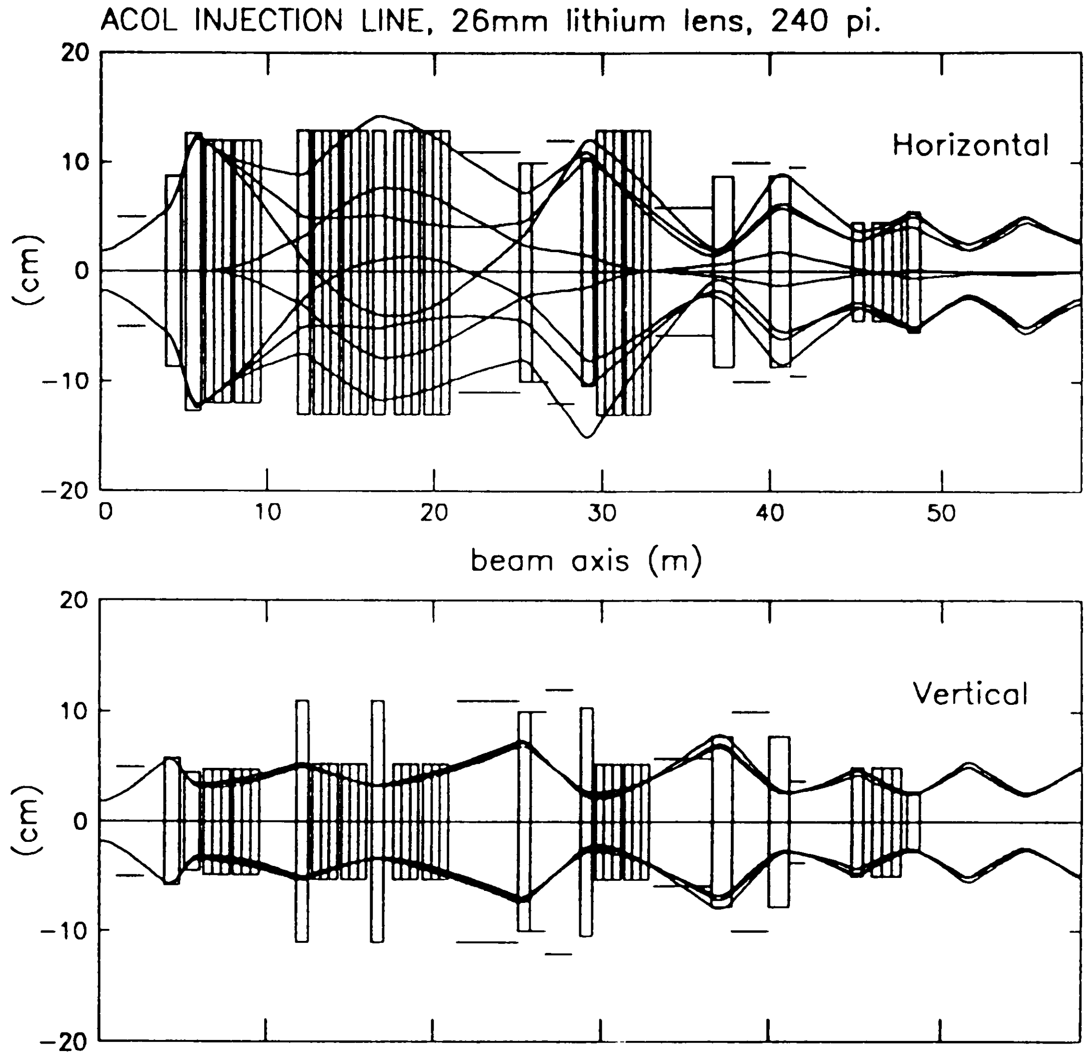

Figure 10: Beam envelopes for ϕ36mm lithium lens injection line optics. See figure 12 for details.

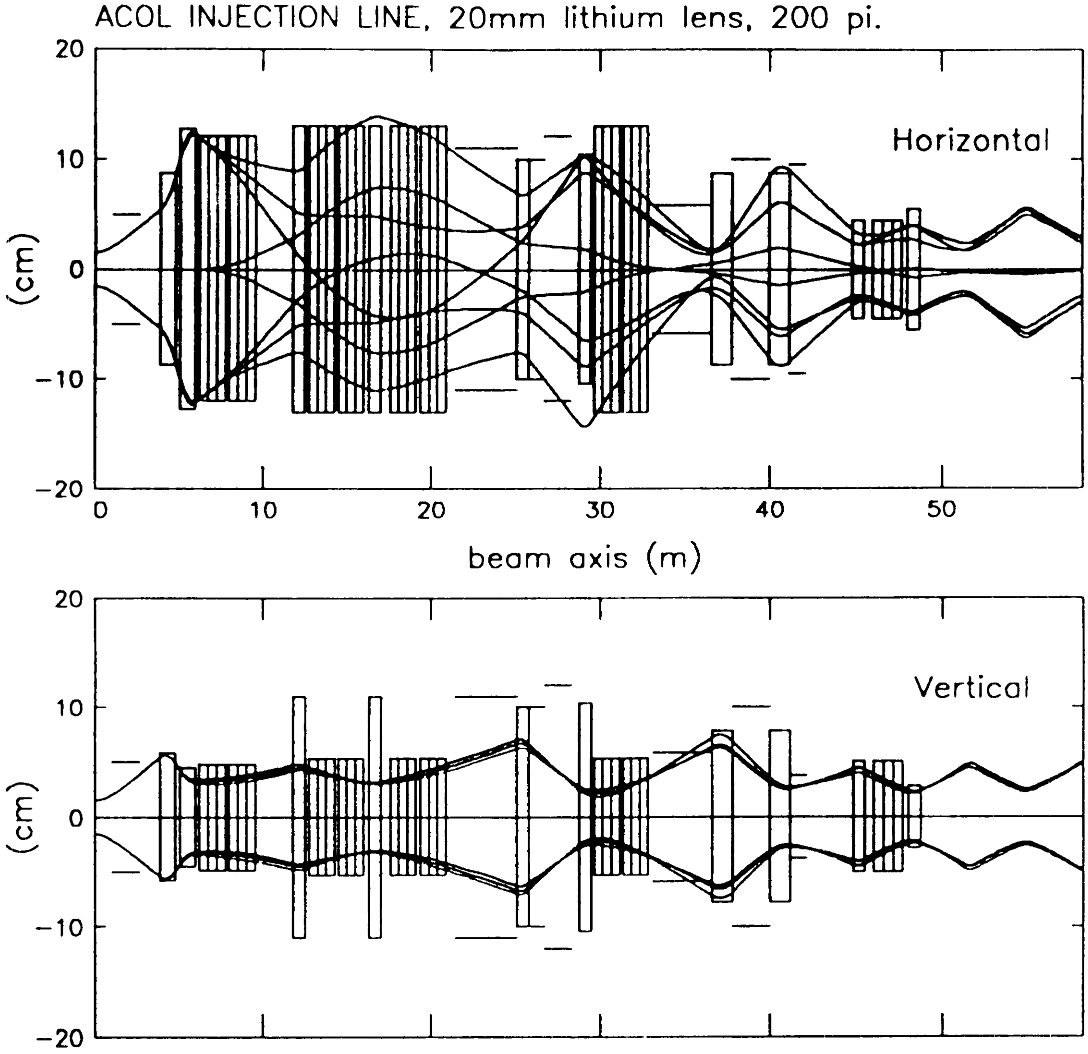

Figure 11: Beam envelopes for 20mm lithium lens injection line optics. See figure 12 for details.

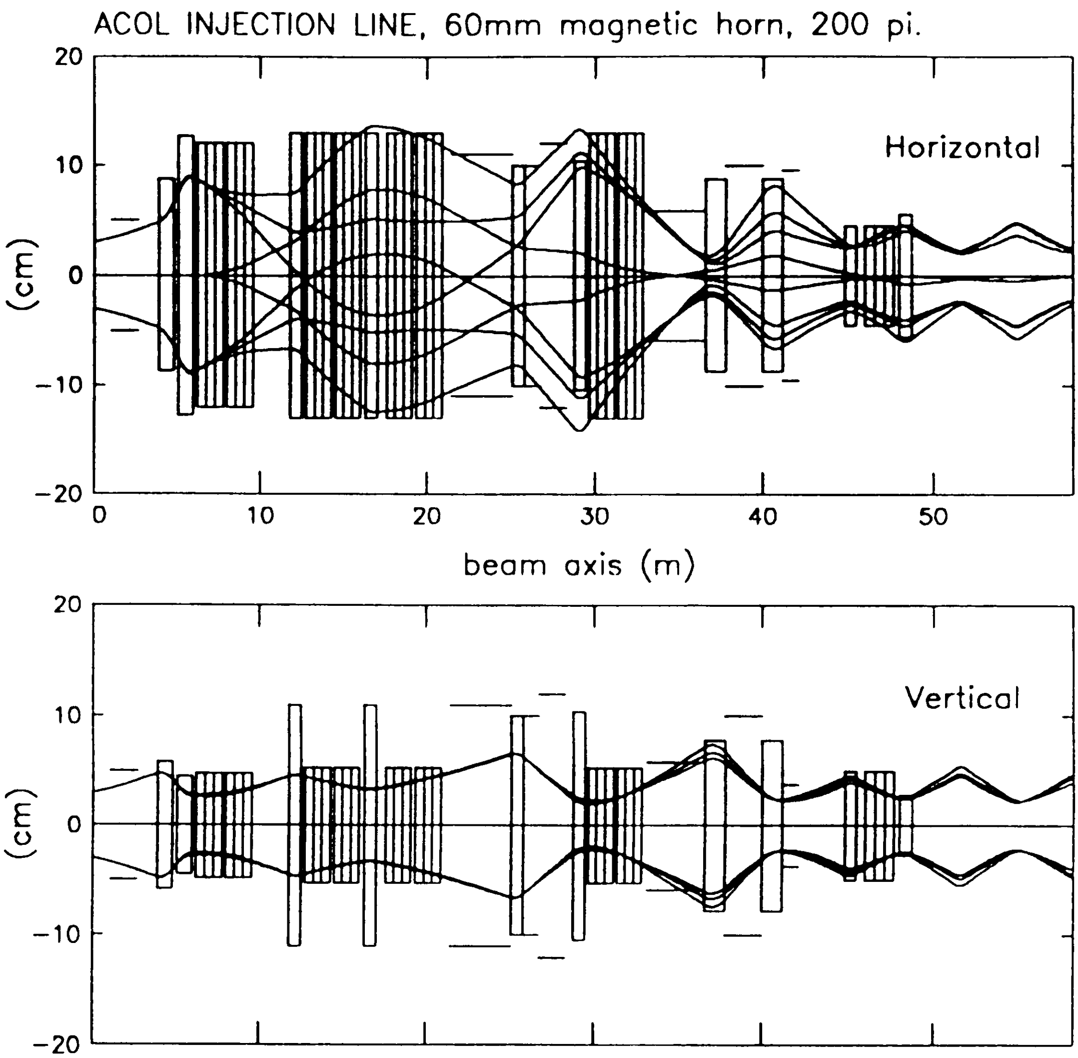

Figure 12: Beam envelopes for 60mm magnetic horn injection line optics. Three beam envelopes are overlapped, corresponding to $\Delta p/p = 0\%, \pm 3\%$. The vertical length of each magnet element (represented by either a plane rectangle for a quadrupole, or a rectangle with three vertical bars for a dipole), indicates the aperture restriction. Vacuum pipes are represented by horizontal lines. The left hand edge is defined as the exit of the collector lens, while the right hand edge is the midpoint of QDN01.

REFERENCES.

1. T.R. Sherwood and S.B. Hancock, private communication.

2. C.D.Johnson *et al*, **Antiproton yield expectations for the AAC project**, IEEE Trans. Nucl. Sci, vol. NS – 48, No. 5, p. 1234 (1987).

3. G. Dugan, **Comparisons of yield calculations with data**, Fermilab Pbar note #448, 1986.

4. K.L.Brown *et al*, **TRANSPORT a computer program for designing charged particle beam transport systems**, SLAC – 91, Rev.2, UC – 28, 1977.

5. T.R. Sherwood, private communication.

6. E.J.N.Wilson (editor), **Design study for an antiproton collector for the antiproton accumulator (AAC)**, CERN/83 – 10 (1983).

7. C.D. Johnson *et al*, **Injection into the new antiproton accumulator complex**, IEEE trans. Nucl. Sci., vol. NS – 32, No. 5, p. 3000 (1985).

8. S. Maury, private communication.

9. P. Sievers *et al*, **The results of prototype tests and temperature and field computations of the CERN lithium lenses**, Proc. of the 13th Int. Conf. on High Energy Accel., p. 272 (1986)

10. J.C. Schnuriger, private communication.

11. P. Sievers *et al*, **Performance and operational experience with CERN – lithium lenses**, (1988).

12. A. Ijspeert, **Development of an aluminium lens**, CERN SPS/ABT/87 – 34

13. B. Autin *et al*, **Performance of the CERN Antiproton Accumulator Complex**, to be published in the Proc. of the European Part. Accel. Conf., Rome (1988).

14. P. Krejcik, private communication.